Validation of a smart structural concept for wing-flap camber morphing

Rosario Pecora[*1], Francesco Amoroso[1a], Gianluca Amendola[1b] and
Antonio Concilio[2c]

[1]*Department of Aerospace Engineering, University of Naples "Federico II", Via Claudio, 21 -80125- Napoli, Italy*
[2]*Smart Structures Laboratory, Italian Aerospace Research Center (C.I.R.A. S.c.p.A.), Via Maiorise -81043-Capua (CE), Italy*

Abstract. The study is aimed at investigating the feasibility of a high TRL solution for a wing flap segment characterized by morphable camber airfoil and properly tailored to be implemented on a real-scale regional transportation aircraft. On the base of specific aerodynamic requirements in terms of target airfoil shapes and related external loads, the structural layout of the device was preliminarily defined. Advanced FE analyses were then carried out in order to properly size the load-carrying structure and the embedded actuation system. A full scale limited span prototype was finally manufactured and tested to:
• demonstrate the morphing capability of the conceived structural layout;
• demonstrate the capability of the morphing structure to withstand static loads representative of the limit aerodynamic pressures expected in service;
• characterize the dynamic behavior of the morphing structure through the identification of the most significant normal modes.
Obtained results showed high correlation levels with respect to numerical expectations thus proving the compliance of the device with the design requirements as well as the goodness of modeling approaches implemented during the design phase.

Keywords: smart structure; morphing; camber variation; wing flap; regional aircraft; FE simulations; experimental tests

1. Introduction

Morphing is one of the new frontiers of aeronautics, although the idea of changing the wing shape or geometry is actually far from being new. The Wright Flyer, the first heavier than air aircraft with an engine, enabled roll control by changing the twist of its wing using cables actuated directly by the pilot. The increasing demand for higher cruise speeds and payloads led to more rigid aircraft structures, that are unable to adapt to different aerodynamic conditions characterizing

---

∗Corresponding author, Assistant Professor, E-mail: rosario.pecora@unina.it
[a] Senior Researcher
[b] Ph. D. Student
[c] Senior Researcher and Laboratory Director

a typical mission profile. The deployment of conventional flaps or slats on a commercial airplane changes the geometry of its wings: however, due to their concentrated nature, they produce discontinuities, sharpening of the geometry and worsening the aerodynamic efficiency. The wings are designed as a "compromise" geometry that allows the aircraft to fly at a range of flight conditions, but the performance at each condition is likely sub-optimal. Moreover, these examples of geometry changes are limited, with narrow benefits compared with those that could be obtained from a wing that is inherently deformable and -globally or locally-adaptable (from aerodynamic performance enhancement (Botez *et al.* 2007) up to aerodynamic noise reduction (Scarselli *et al.* 2010), load control capabilities and consequent optimization of the structural weight). The ability of a wing surface to change its geometry during flight has interested researchers and designers over the years (a quite thorough survey may be found in Barbarino *et al.* 2011a): an adaptive wing indeed diminishes the compromises required to ensure the operation of the airplane in multiple flight conditions (Stanewsky 2001).Novel strategies have been considered in the last decade: for example, the idea of producing smooth variations of the geometry even in presence of large displacements distributed over a wider portion of the wing, is well documented (Chopra 2002,Vasista*et al.* 2012). This approach, however, gives rise to an interesting paradox: the same structure that has to withstand the external aerodynamic loads without suffering appreciable deformations, has to dramatically change its shape to fit the best current flight condition. Several international researchers have been working on this topic by following different methods to significantly modify specific wing parameters (e.g., upper skin curvature -to delay the appearance of the laminar transition point- (Grigorie, Botez *et al.* (2012a), Grigorie, Botez *et al.* (2012b)), local or global camber (Spillman 1992, Wildschek *et al.* 2008, Bilgen *et al.* 2009, Barbarino *et al.* 2009, Ameduri *et al.* 2012), wing span (Blondeau and Pines 2004, Bye and McClure 2007, Ivanco *et al.* 2007) or twist (McGovan *et al.* 1999, Pecora *et al.* 2012) to achieve better aerodynamic performance. Some efforts have been focused on the development of kinematic chains (Popov *et al.* 2010, Pecora *et al.* 2011, Song *et al.* 2011), others on the development of compliant structures (Monner *et al.* 1999, Barbarino *et al.* 2011b). Among these latter, the adoption of a Variable Geometry Truss (VGT) concept as primary load carrying structure is quite widespread (Barbarino *et al.* 2007, Baker and Friswell 2008, Hasse and Campanile 2009).Compliant structures are designed to achieve large deformations by relying only upon elastic deformation of their structural components. This requires the balance between high load-carrying capabilities to sustain external forces on the one side, and sufficient flexibility to realize the target shape smoothly under the actuation forces on the other. Compared to compliant structures, rigid-body mechanisms offer a direct solution to the morphing paradox. Actuation is carried out via a lever mechanisms driven by load-bearing actuators combing load carrying and actuation functions. Fewer actuators are typically required to control the morphing process whose overall benefit expected on the system level drives the additional mass, volume, force and power required by the actuation system.

Within the framework of the JTI-Clean Sky project (www.cleansky.eu),the authors focused on the design and technological demonstration of a novel architecture enabling the camber variation of a flap segment to be installed on next generation open rotor green regional aircraft (CS-25 category); the driving idea was to replace a conventional double slotted flap with a single slotted morphing flap in order to improve aircraft high lift performances -in terms of maximum attainable lift coefficient and stall angle- as well as to reduce the noise emitted by the high lift system.

Studies were limited to a portion of the flap element obtained by slicing the actual flap geometry (0.62 meters chord) with two cutting planes distant0.8 meters along the wing span. Target morphed shapes were evaluated on the base of 2D CFD optimization analyses (Mingione

2010) and were provided to the authors as input data for the design activities described in this paper. A structural concept was then assessed in order to ensure the reversible transition from the nominal to the target shape of the flap segment. Advanced finite element models were elaborated to support the structural design; numerical models reliability as well as the overall structural concept functionality and performances were finally proved through experimental tests on a full-scale test article.

2. Morphing architecture, general concept

Referring to the unmorphed and morphed airfoils of the flap element depicted in Fig. 1, the conceptual layout of an articulated (*finger-like*) rib structure was assessed in order to physically realize the transition from the baseline airfoil configuration to the target one.

The rib structural concept (Fig. 2) is characterized by four main plates: *B0*, *B1*, *B2* and *B3*. *B0* and *B2* have the same middle plane; *B1* and *B3* are staggered respect to them sharing always a common middle plane. Each plate is connected to the adjacent one by a hinge located on rib camber line (points *A*, *B* and *C,* respectively at 20%, 50% and 70% of rib chord).

Plate *B0* is linked to plate *B2* by means of a rod element hinged at points *D* and *E*, hinges *D* and *E* being respectively located on *B0* and *B2*. Plate *B1* is linked to plate *B3* through a second rod hinged at points *F* and *G*.

Crossed links (DE and FG) positions have been conceived in order to assure specific rotation ratios between adjacent plates and an overall plates movement useful to match the target morphed shape. More in detail, considering plate *B0* fixed on flap strut, a downward rotation of *B1* around *A* by an angle of 3° makes all the other plate to move so that the final positions of hinges *B* and *C* (marked with a * in Fig. 2) are on the camber line of the morphed airfoil. Same applies if 11° downward rotation is imposed to plate *B2* around *B* or 3° downward rotation is imposed to plate *B3* around *C*. Generally speaking, the rib architecture represents a single degree-of-freedom system; if a single plate is moved by a unique actuator, all the other plates are driven to move in compliance with the final shape to be achieved.
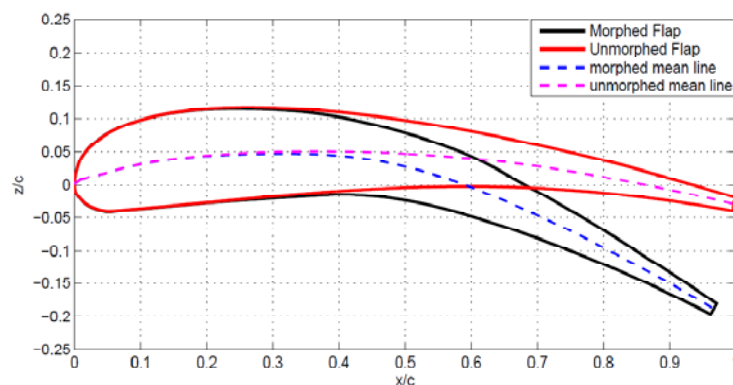

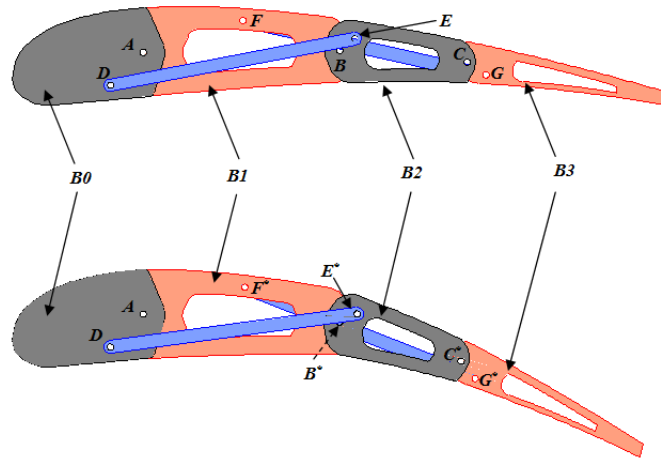Fig. 1 Flap airfoil: nominal geometry (unmorphed shape) amd target geometry (morphed shape)

Fig. 2 Morphing rib layout (unmorphed and morphed configurations)
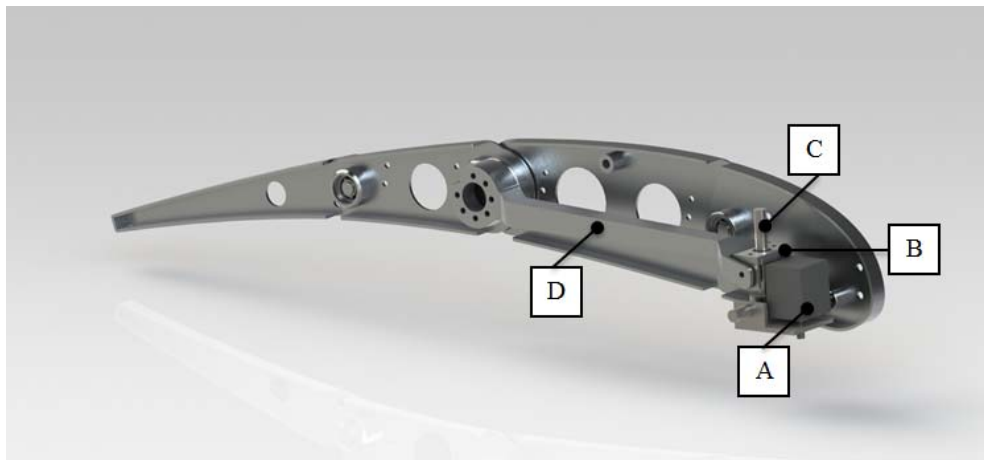

Fig. 3 Actuation concept

In order to increase the structural stiffness of the rib with respect to the torque moment induced by the aerodynamic loads, the actuator was installed on plate B0 and connected to plate B2 through a robust transmission chain (Fig. 3). A conventional stepper motor was selected as actuator (Fig. 3, A). A gear box was used to convert the rotation of the motor shaft into the sliding of a cursor (Fig. 3, B) along an endless screw (Fig. 3, C); the movement of the cursor is then transferred to the plate B2 by means of a stiff beam (Fig. 3, D) rigidly connected to such rib segment.

The spanwise stiffness of the flap structure was assured by a typical box arrangement (Fig. 4) characterized by:

- 0.4 meters span (i.e.,: two bays, three morphing ribs for the overall flap segment);
- two spars connecting plates B0/B1/B2 of two consecutive ribs;
- one spar connecting plates B3 of two consecutive ribs.

In order to allow spars riveting on ribs plates, the crossed links of each rib were shifted along the span (Fig. 5) and suitably installed to pass through spars holes.

A segmented skin solution was adopted. Each box was covered by a conventional metallic skin properly riveted along spars and ribs' plates; in proximity of the hinges connecting consecutive ribs plates (and therefore consecutive boxes), the skin panels installed on the forward box were assumed to slide on the ones installed on the rearward box, thus generating an *armadillo like* covering structure.

AL2024 alloy was considered for ribs plates, spars and stringers; steel was used for crossed links and their supporting rods, as well as for some components of the actuation chain.
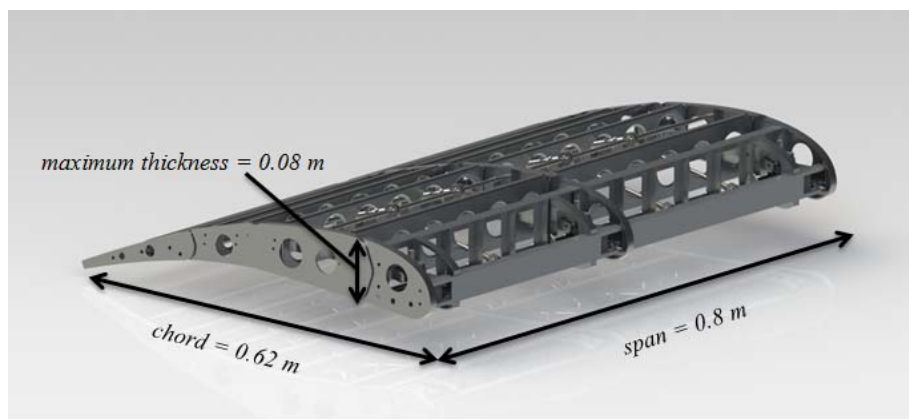

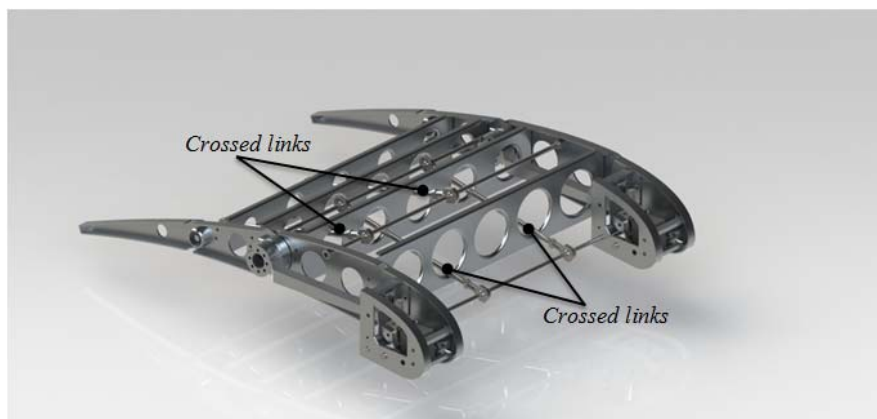Fig. 4 Morphing architecture of the flap segment and overall dimensions

Fig. 5 Crossed links installation (some structural components have been hidden for clarity)

3. Morphing architecture, finite element analysis

In order to verify the structural robustness of the conceived morphing architecture as well as to estimate its dynamic behavior, a very refined finite element model (FEM) was generated (Fig. 6). Ribs and spar were meshed using CTRIA and CQUAD elements; TET4 elements were adopted for the actuation beam while mono-dimensional elements (BEAM type) were considered for the crossed links and their supporting structure. All the hinges were modeled by means of two-nodes CBUSH elements (see MSC-MD/NASTRAN® Reference Manual); each node of the CBUSH was rigidly connected to a representative set of nodes belonging to the hinged items' elements (Fig. 7).
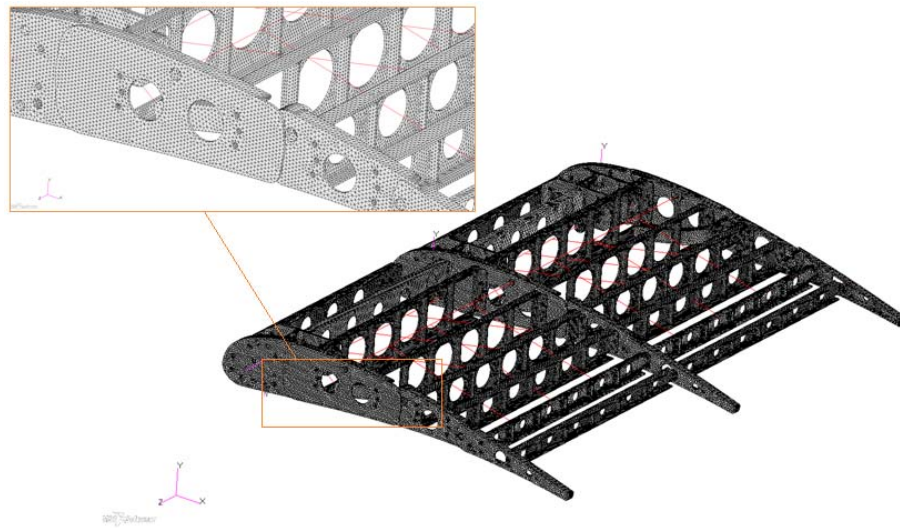
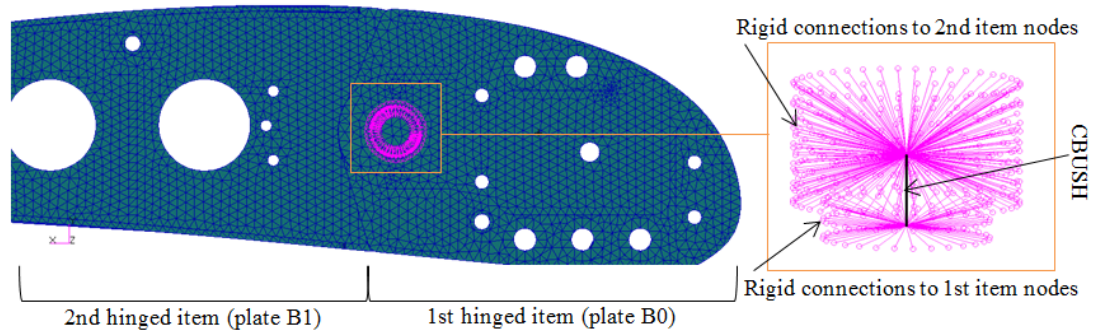Fig. 6 Morphing flap, finite element model (skin hidden)

Fig. 7 Hinge model

Due to the segmented solution adopted for the skin (see paragraph 2), it was decided to avoid the modelling of the skin thus conservatively neglectingits contribute to the overall stiffness of the load-carrying structure.

The finite element model was considered constrained in correspondence of the first plate of the external ribs (leading edge) and actuator shaft rotation was prevented (clamped actuators configuration).

The following analyses were carried out using MSC/MD-NASTRAN® solver:
- Linear static analysis;
- Modal analysis.

For what regards static analyses, the highest load distribution expected in service was taken in account (33° flap deflection, 4° aircraft leading angle, 73 m/s flight speed @ sea level).

As expectable, maximum Von Mises stresses was detected around the hinges of the central rib (Fig. 8(a))); the obtained value (≈ 83 MPa) resulted however satisfactory below the yield strength of the rib plates material (AL2024 alloy). High safety margins were also obtained with respect to the buckling of rib plates, spar webs and crossed links beams.The central rib was moreover characterized by the highest elastic displacements (Fig. 8(b)); on each plate of the central rib, maximum displacements occurred in correspondence of the nodes located on the lower surface at the most rearward chordwise position (i.e.,: lower tip of rib plates). Maximum displacements along central ribs plates have been recapped in Table 1.
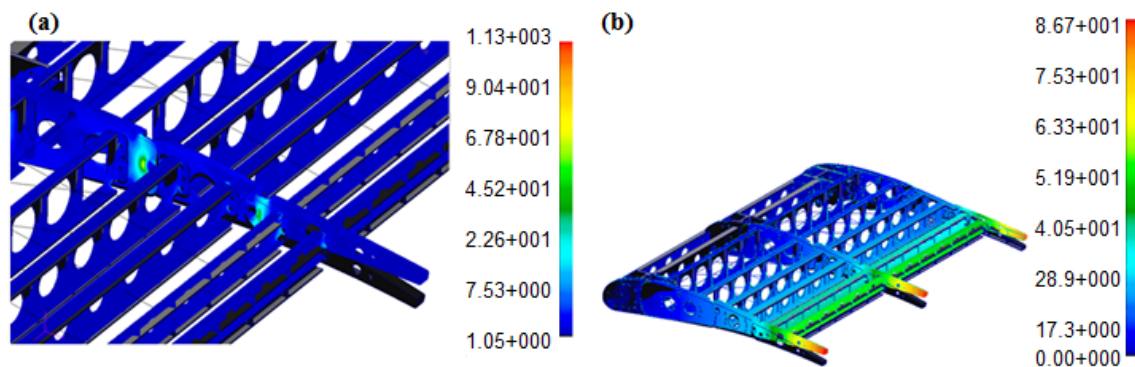

Fig. 8 Static analysis results: (a) Von Mises stress contour (MPa) and (b) Displacements contour (mm)

Table 1 Maximum (elastic) displacements along central rib chord

Node Position	(Elastic) Displacement at Node [mm]
Central rib, lower tip of the 1st plate	-1.0
Central rib, lower tip of the 2nd plate	-21.5
Central rib, lower tip of the 3rd plate	-44.0
Central rib, lower tip of the 4th plate	-75.5

Normal modes were evaluated in the frequency range 0 Hz-80 Hz[•] referring to Lanczos method.

Only two modes were detected in the investigation range:

- a *morphing mode*, resembling to the morphed shape of the flap and mainly due the elasticity of the actuation chain;
- a *torsion mode* characterized by a nodal line in correspondence of the central rib.

Natural frequencies and modes shapes have been respectively reported in Table 2 and Fig. 9.

Table 2 Normal modes frequencies (Actuators clamped, frequency range 0 Hz -80 Hz)

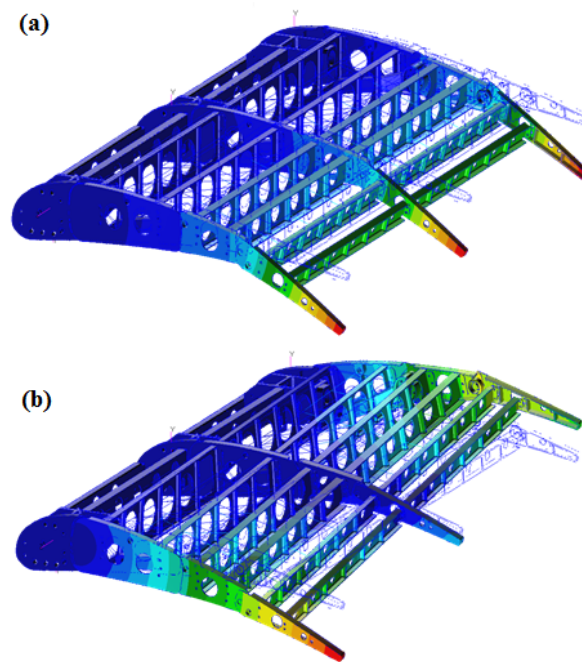|	**Mode Number**	**Mode Name**	**Frequency [Hz]**
-Actuators clamped-	1	*Morphing mode*	9.84
Frequency range: 0Hz-80Hz	2	*Torsion*	21.87

Fig. 9 Normal modes shapes, (a) *morphing mode* and (b) *torsion mode*

[•]The upper limit of the frequency range was chosen in order to detect all elastic modes believed to be significant from the aeroelastic standpoint.

4. Morphing architecture, experimental tests

A prototype of the flap segment (Fig.) described in paragraph 2was manufactured and used as test article (T/A) for an experimental test campaign aimed at :

- demonstrating the morphing capability of the conceived structural layout;
- demonstrating the capability of the morphing structure to withstand static loads representative of the limit aerodynamic pressures expected in service;
- characterizing the dynamic behavior of the morphing structure through the identification of the most significant normal modes.

According to the scope of the experimental campaign, it was intentionally decided to not provide the T/A with skin. Such decision was driven by the following considerations:

- *Absence of skin effects on flap morphing capabilities*; due to the conceived structural arrangement and coverage segmentation (see paragraph 1), skin would have not produced any relevant effects on flap morphing capabilities; no additional actuation force would have been in fact required to morph the skin.
- *Inner structure accessibility during tests*; the inner structure should have been accessible during tests thus allowing a direct inspection of the main structural components as well as of the actuation system.
- *Unrealistic skin installation*; in order to assure the accessibility of the inner structure during tests, skin should have been easily removable; rivets should have been therefore replaced by bolts or screw thus leading to an unrealistic skin installation. Moreover, the need for bolts/ screws holes would have led to an unreasonable increase of structural components thickness.
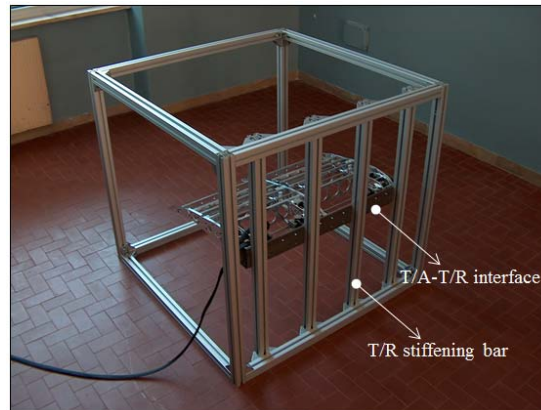

Fig. 10 Morphing flap prototype

Fig. 11 Test article and test rig

The T/A was installed on a cubic test rig (T/R) delimited by twelve Aluminium bars (1.10 m length) and properly stiffened at T/A anchorage points through four extra bars (Fig. 11). A C-shaped steel beam was used as T/A – T/R interface; the T/A was rigidly fixed to the interface through screws bolted to the leading edge blocks of the external ribs only (central rib not connected to the interface). The interface was then bolted to rig in correspondence of the vertical stiffening bars.

In order to better organize the test data, a common reference system S_0 was considered for all experimental measurements; the following definition applies to S_0 (Fig. 12):
- Origin on the upper side of the central rib at the mid chord of the leading edge block;
- X-axis parallel to the ground and oriented towards T/A trailing edge;
- Y-axis along T/A span and positively oriented toward the RT rib;
- Z-axis perpendicular to the ground and upward oriented.
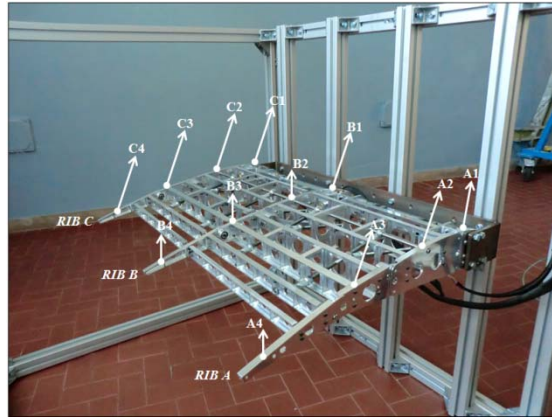

Fig. 12 S_0 reference system

Fig. 13 Ribs and Ribs' plates nomenclature

A suitable nomenclature was adopted for T/A ribs and ribs' plates thus enabling a rational and univocal identification of measurement/acquisition points on T/A structure (Fig. 13).

4.1 Functionality tests

Functionality tests were carried out to give evidence of flap morphing capability in terms of:
- Matching of target morphed shape;
- Controllability of morphing evolution.

The following step-by-step test procedure was used.

Step 1-*Definition of acquisition points for Z-displacements measurement along B-Rib chord*.
Three acquisition points were defined at the upper tip of the plates B2, B3, B4 (points F,G,H, Fig. 14(a)). Due to the high bending stiffness of the T/A, it was considered unnecessary to add acquisition points also along rotating segments of ribs A (A2,A3,A4) and C (C2,C3,C4).

Step 2-*T/A morphing*.
Referring to T/A morphing cinematic, a specific angular velocity time history was (synchronously) assigned to the three stepper motors actuating the three ribs. The action of the stepper motors was automatically driven by an open-loop control algorithm implemented in PLC language and running in MS-Windows® environment.

Step 3-*Measurement of Z-displacements at acquisition points*.
At the end of the morphing evolution (determined by stepper motors automatic arrest), Z-displacements were measured at acquisition points; the measurements were performed through a laser head sliding along a reference (horizontal) bar installed at the top of the rig[•] (Fig. 14(b)).

[•]For the generic acquisition point i (i=F,G,H) the vertical distance from the reference bar was measured both in un-morphed (d_i)and morphed configurations (d_i*); the Z-displacement of the acquisition point was then obtained as $\Delta Z_i = d_i - d_i$*.
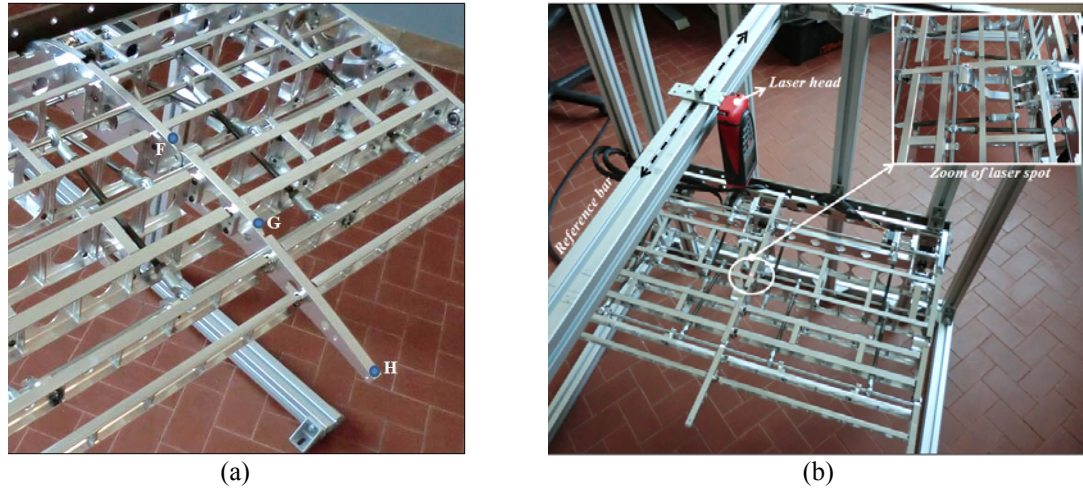
Fig. 14 (a) Acquisition points for Z-displacements and (b) Measurement system based on sliding laser head

Step 4 - *T/A un-morphing.*

The un-morphed shape was restored by (synchronously) reversing stepper motors rotation according to the same velocity time histories of step 2.

Steps 2,3,4 were repeated two times in order to prove the stability (and the full controllability) of the morphing cinematic. Morphed shape matching was appreciated by comparing the experimentally measured Z-displacements with their design values (Table 3).

According to the results recapped in Table 3, the conceived architecture proved to be extremely reliable in producing stable and controllable morphing compliant with design requirements. Unmorphed / morphed shapes reproduced during tests have been reported in Fig. 15.

Table 3 Z-Displacements comparison

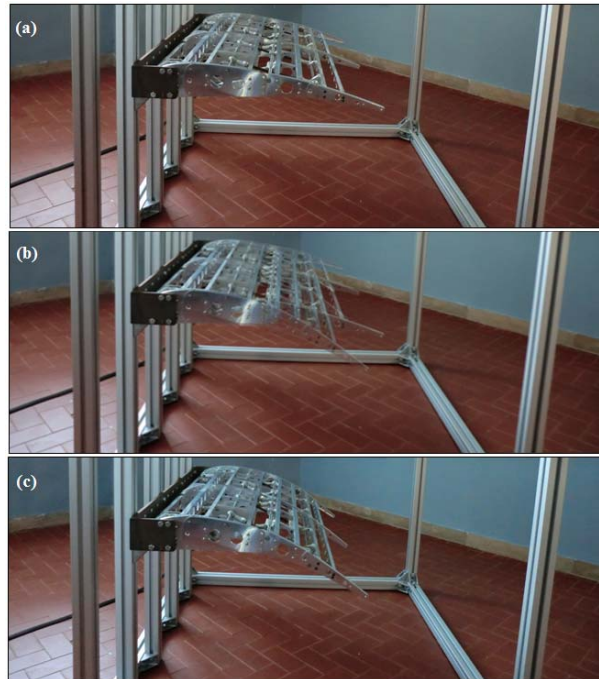|	Z-DISPLACEMENTS [mm]		
Point	Design Value	Experimental Value (1st measurement)	Experimental Value (2nd measurement)
F	-12.3	-12.0	-12.5
G	-42.0	-42.0	-42.0
H	-78.7	-79.0	-78.5

Fig. 15 T/A morphing: (a) unmorphed shape, (b) unmorphed & morphed shapes overlapped and (c) morphed shape

4.2 Static test

Static test was carried out to give evidence of flap capability in withstanding design loads without failures and/or local plasticization.

The T/A was mounted in upside-down un-morphed configuration (upper surface toward the ground) and gradually loaded through sandbags of 2 Kg weight each. The number of sandbags along each chordwise portion of the T/A chord was chosen in order to reproduce the limit load condition expected in service (see paragraph 3).

(Elastic) Z-displacements were measured in correspondence of the acquisition points E',F',G',H'[•] located at the lower surface of the central rib at the most rearward chordwise position of each plate (Fig. 16); the same measurement system described in paragraph 4.1 was used.

The T/A was then gradually unloaded by removing all sandbags and the full recovery of un-deformed shape was observed (Table 4 and Fig. 17).

Neither failures nor local plasticization were detected.

[•] The choice of the acquisition points was made by taking in account that, on the base of numerical simulations described in paragraph 3, the highest elastic displacements were expected to arise along central rib chord.

Fig. 16 Acquisition points for (elastic) Z-displacements

A functional test was finally carried out and it was shown that T/A functionality resulted unaffected by static loading procedure (Z-displacements at points F,G,H resulted equal to the ones reported in Table 3, paragraph 4.1).

Actuation of morphing structure was also performed in presence of sandbags and the T/A capability to preserve the desired morphed shape under applied loads was successfully proven.

Table 4 (Elastic) Z-displacements along central rib chord

Point	(Elastic) Z-Displacements [mm] (loads application)	(Elastic) Z-Displacements [mm] (loads removal)
E'	-1.0	1.0
F'	-24.0	24.5
G'	-47.0	47.0
H'	-70.5	70.0

Fig. 17 Static test: (a) no load applied, (b) loaded structure and (c) un-loaded structure

4.3 Ground Vibration Tests (GVT)

GVT were carried out according to the test matrix reported in the following table.

Free-free condition was reproduced by anchoring the T/A to the T/R through soft springs linked to rib blocks A1 and C1 (Fig. 18). For all GVT tests, the structure was excited through hammer impact (along –Z- direction) at the upper surface of rib block C3. Accelerometers time-responses (along +Z-direction of S_0) were acquired in correspondence of 12 reference points over the T/A (Fig. 19).

Table 5 Ground Vibration Test (GVT) matrix

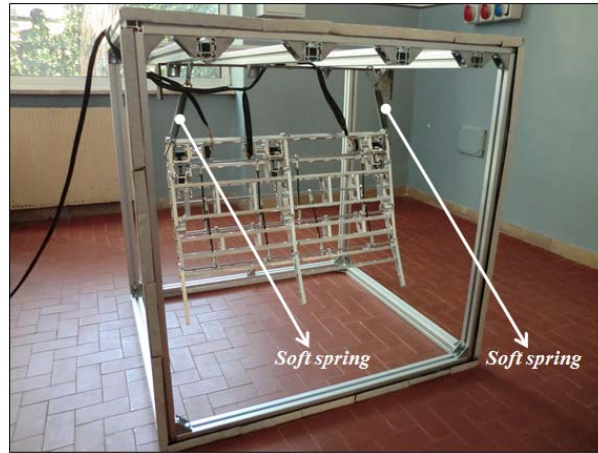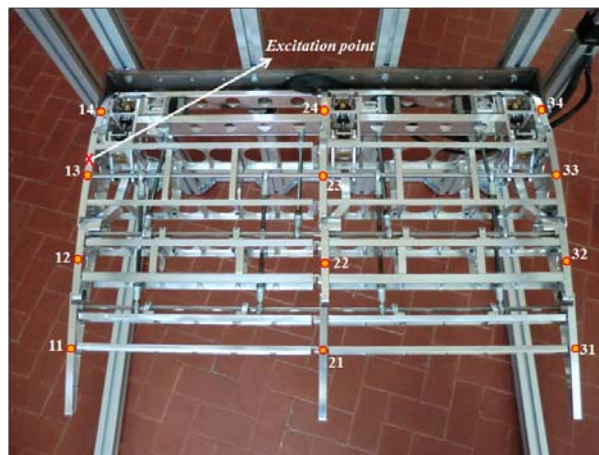| GVT	T/A Constraint Condition	T/A Configuration	GVT Scope
A-1	Fixed to the T/R	Un-morphed	*morphing mode*
A-2	(as illustrated in par. 4, Fig. 11)	Morphed	identification
B	Free-free	Un-morphed	normal modes identification (frequency range 0-80 Hz)

Fig. 18 T/A in free-free condition

Fig. 19 Excittation and acquisition points

For GVT A-1 and A-2 only, the T/R was loaded with 12 sandbags (3 sandbags on each upper side of the rig, total added mass equal to 24 Kg) to lower its first frequency thus avoiding significant T/R influence on the morphing mode frequency. Frequency response functions (FRF) were synthetized through LMS-SCADAS-305® facilities by averaging over five measurements per acquisition point; a sample frequency of 160 Hz was used with a resolution of 0.156 Hz (number of FRF spectral lines equal to 512).

Modal parameters (frequency, Z-displacements, damping) were finally identified in the frequency range 0-80 Hz. Obtained results have been recapped in Table 6 and therein recalled figures.
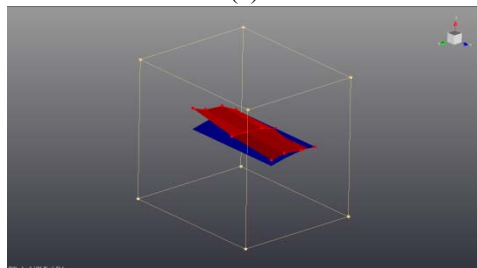
Table 6 Experimental modes

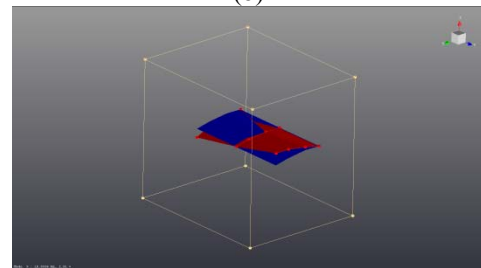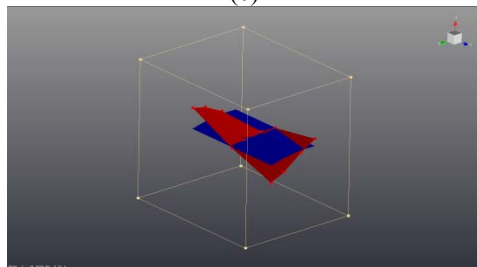| Test	Mode Number	Mode Name	Frequency [Hz]	Modal Damping [%]	Modal Shape (Figure)
GVT A-1	1	*Morphing mode*	9.21	1.41	Fig. 20 (a)
	2	*Torsion*	18.80	1.01	Fig. 20 (b)
GVT A-2	1	*Morphing mode*	9.14	2.89	Fig. 20 (c)
	2	*Torsion*	19.03	2.91	Fig. 20 (d)
GVT B	1	*Torsion*	20.94	0.91	Fig. 20 (e)
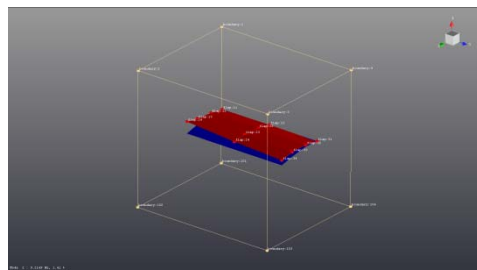
(a)
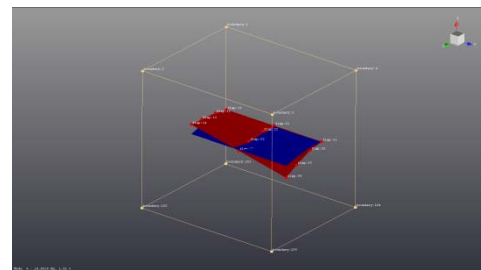
(b)

(c)

(d)

(e)

LEGEND
Undeformed shape
Modal shape

Fig. 20 Experimental modes shape

For GVT A-1 and A-2 two modes were identified: the *morphing mode* and a *torsion mode* characterized by a nodal line along the central rib; no significant variation of modal parameters was observed between un-morphed (A-1) and morphed (A-2) configurations thus proving the absence of morphing influence on the dynamic behavior of the flap.

In free-free conditions the morphing mode resulted outside the range of practical interest (0-80Hz) and the torsion mode occurred at a slightly higher frequency due to the fixed constraints removal at blocks A1 and C1; in such a constraint condition, the nodal line along the central rib is still present and a new nodal line appears in correspondence of the hinges connecting the first and the second blocks of all ribs.

5. Conclusions

In the framework of JTI-Clean Sky project, authors investigated a high TRL solution for a morphing flap element to be implemented on a real-scale regional transportation aircraft. On the base of specific aerodynamic requirements in terms of target shapes and related external loads, the structural layout of the device was preliminarily defined. Advanced finite element analyses were then carried out in order to properly size the load-carrying structure and the actuation system. A full scale limited span prototype was finally manufactured and tested to:

- d demonstrate the morphing capability of the conceived structural layout;
- demonstrate the capability of the morphing structure to withstand static loads representative of the limit aerodynamic pressures expected in service;
- characterize the dynamic behavior of the morphing structure through the identification of the most significant normal modes.

Rational approaches were implemented in an efficient test campaign providing the necessary database for the mechanical demonstration of the morphing structure.

Test outcomes showed that:

- reliable and stable morphing compliant with design requirements is assured by the device both in absence and in presence of applied external loads (representative of limit pressure distribution expected in service);
- normal modes result unaffected by architecture's settings (morphed/unmorphed) and related parameters (frequency/damping/shape) do not give rise to specific concerns of aeroelastic nature.

Moreover, good correlation levels with respect to numerical expectations were observed both in terms of static deflections under applied loads (see Table 1 paragraph 3 and Table 4, paragraph 4.2) and modal parameters (see Table 2, paragraph 3 and Table 6 paragraph 4.3).

The slight difference between numerical and experimental results was mainly imputed to difficulties in simulating the local flexibility of hinges and constraints; this inevitably led to a slightly stiffer numerical model. On the other hand, since the deviation from experimental outcomes resulted negligible from a practical standpoint, the goodness of modeling approaches implemented during the design phase was considered more than satisfactory.

In force of the extreme reliability and robustness of the designed architecture as well as of the simplicity (and conventionality) of the actuation mechanism enabling shape control, no big efforts are expected to push the prototype towards higher technological standards for in-flight applications. The conceived (and tested) structural arrangement proved also to be extremely versatile and

further improvements may be easily implemented with no impacts on assessed morphing capabilities: from the weight reduction trough the adoption of composite materials, to the introduction of redundant actuators for the safe recovery of standard-flap functionalities in case of in-flight actuators failures or jamming.

Acknowledgements

References

Ameduri, S., Brindisi, A., Tiseo, B., Concilio, A. and Pecora, R. (2012), "Optimization and integration of shape memory alloy (SMA)-based elastic actuators within a morphing flap architecture", *J. Intel. Mat. Syst. Str.*, **23**(4), 381-396.

Baker, D. and Friswell, M.I. (2008), "The design of morphing aerofoils using compliant mechanisms", *Proceedings of the 19th International Conference on Adaptive Structures and Technologies*, Ascona (Switzerland), October.

Barbarino, S., Ameduri, S. and Pecora, R. (2007), "Wing camber control architectures based on SMA: numerical investigation", *Proceedings of SPIE*, **6423**, 64231E-1 - 64231E-8.

Barbarino, S., Bilgen, O., Ajaj, R.M., Friswell, M.I. and Inman D.J. (2011a), "A review of morphing aircraft", *J. Intel. Mat. Syst. Str.*, **22**, 823 -877.

Barbarino, S., Pecora, R., Lecce, L., Concilio, A., Ameduri, S. and Calvi, E.(2009), "A novel SMA-based concept for airfoil structural morphing", *J. Mater. Eng. Perform.*, **18**(5), 696-705.

Barbarino, S., Pecora, R., Lecce, L., Concilio, A., Ameduri, S. and De Rosa, L. (2011b), "Airfoil structural morphing based on S.M.A. actuator series: numerical and experimental studies", *J. Intel. Mat. Syst. Str.*, **22**, 987-1003.

Bilgen, O., Kochersberger, K.B., Inman, D.J. and Ohanian III, O.J. (2009), "Novel, bi-directional, variable camber airfoil via macro-fiber composite actuators", *Proceedings of the 50th AIAA/ASME/ASCE/AHS/ASC Structures, Structural Dynamics and Materials Conference*, Palm Springs (California, US), May.

Botez, R.,M., Molaret, P. and Laurendeau, E. (2007), "Laminar flow control on a research wing project presentation covering three year period", *Canadian Aeronautics and Space Institute Annual General Meeting*, Montreal (Canada), January.

Blondeau, J. and Pines, D. (2004), "Pneumatic morphing aspect ratio wing", *Proceedings of the 45th AIAA/ASME/ASCE/AHS/ASC Structures, Structural Dynamics and Materials Conference*, Palm Springs (California, US), April.

Bye, D.R. and McClure, P.D. (2007), "Design of a morphing vehicle", *Proceedings of the 48th AIAA/ASME/ASCE/AHS/ASC Structures, Structural Dynamics and Materials Conference*, Honolulu (Hawaii, US), April.

Chopra, I. (2002), "Review of state of art of smart structures and integrated systems", *AIAA J.*, **40**(11), 2145-2187.

Grigorie, L.T., Botez, R.,M., Popov, A.V., Mamou, M. and Mébarki, Y. (2012a), "A hybrid fuzzy logic proportional-integral-derivative and conventional on-off controller for morphing wing actuation using shape memory alloy, Part 1: Morphing system mechanisms and controller architecture design", *Aeronaut. J.*, **40** (1179), 433-449.

Grigorie, L.T., Botez, R.M., Popov, A.V., Mamou, M. and Mébarki, Y. (2012b), "A hybrid fuzzy logic proportional-integral-derivative and conventional on-off controller for morphing wing actuation using shape memory alloy, Part 2: Controller implementation and validation", *Aeronaut. J.*, **116**(1179), 451-465.

Hasse, A. and Campanile, L.F. (2009), "Design of compliant mechanisms with selective compliance", *Smart Mater. Struct.*, **18**, 1-10.

Ivanco, T.G., Scott, R.C., Love, M.H., Zink, S. and Weisshaar, T.A. (2007), "Validation of the Lockheed Martin morphing concept with wind tunnel testing", *Proceedings of the 48th AIAA/ASME/ASCE/AHS/ASC Structures, Structural Dynamics and Materials Conference*, Honolulu (Hawaii, US), April.

McGowan, A.R., Horta, L.G., Harrison, J.S. and Raney, D.L. (1999), "Research activities within NASA's morphing program", *Proceedings of the RTO AVT Specialists' Meeting on Structural Aspects of Flexible Aircraft Control*, Ottawa (Canada), October.

Mingione, G. (2010), *Preliminary design of wing trailing edge morphing architectures*, JTI-GRA deliverable no. GRA2.2.1-TN-CIRAPlus-TECH-210105A, (research report).

Monner, H.P., Sachau, D. and Brietbach, E. (1999), "Design aspects of the elastic trailing edge for an adaptive wing", *Proceedings of the RTO AVT Specialists' Meeting on Structural Aspects of Flexible Aircraft Control*, Ottawa (Canada), October.

MSC-MD/NASTRAN ®, Software Package, Ver. R3-2006, "Reference Manual".

Pecora, R., Amoroso, F. and Lecce, L. (2012), "Effectiveness of wing twist morphing in roll control", *J. Aircraft*, **49**(6), 1666-1674.

Pecora, R., Barbarino, S., Concilio, A., Lecce, L. and Russo, S. (2011), "Design and functional test of a morphing high-lift device for a regional aircraft", *J. Intel. Mat. Syst. Str.*, **22**, 1005-1023.

Popov, A.V., Grigorie, T.L., Botez, R.M., Mébarki, Y. and Mamou, M. (2010), "Modelling and testing of a morphing wing in open-loop architecture", *J. Aircraft*, **47**(3), 917-923.

Song, G., Ma, N., Li, L., Penney, N., Barr, T., Lee, H.J. and Arnold, S. (2011), "Design and control of a proof-of-concept active jet intake using shape memory alloy actuators", *Smart Struct. Syst.*, **7**(1), 1-13.

Scarselli, G., Marulo, F. and Paonessa, A. (2010), "Sensitivity investigation of aircraft engine noise to operational parameters", *Proceedings of the 16th AIAA/CEAS Aeroacoustics Conference (31st AIAA Aeroacoustics Conference)*, Stockholm (Sweden), June.

Spillman, J. (1992), "The use of variable camber to reduce drag, weight and costs of transport aircraft", *Aeronaut. J.*, **96**, 1-8.

Stanewsky, E. (2001), "Adaptive wing and flow control technology", *Prog. Aerosp. Sci.*, **37**, 583-667.

Vasista, S., Tong, L. and Wong, K.C. (2012), "Realization of morphing wings: a multidisciplinary challenge", *J. Aircraft*, **49**, 11-28.

Web site link: www.cleansky.eu (Web site of the European Community project funding the researches described in this paper).

Wildschek, A., Grünewald, M., Maier, R., Steigenberger, J., Judas, M., Deligiannidis N. and Aversa, N. (2008), "Multi-functional morphing trailing edge device for control of all-composite, all-electric flying wing aircraft", *Proceedings of the 26th Congress of International Council of the Aeronautical Sciences (ICAS)*, Anchorage (Alaska, US), September.

CC